

Ultra Fast Astronomy: Optimized Detection of Multimessenger Transients

Mikhail Denissenya¹, Eric Linder^{1,2}

¹*Energetic Cosmos Laboratory, Nazarbayev University, Nur-Sultan 010000, Kazakhstan*

²*Berkeley Center for Cosmological Physics & Berkeley Lab,
University of California, Berkeley, CA 94720, USA*

(Dated: January 11, 2021)

Ultra Fast Astronomy is a new frontier becoming enabled by improved detector technology allowing discovery of optical transients on millisecond to nanosecond time scales. These may reveal counterparts of energetic processes such as fast radio bursts, gamma ray bursts, gravitational wave events, or play a role in the optical search for extraterrestrial intelligence (oSETI). We explore three science cases and their optimization under constrained resources, basically how to distribute observations along the spectrum of short duration searches of many targets or long searches over fewer targets. We present some analytic and some numerical optimizations, of both raw detections and science characterization such as a Fisher information analysis of constraining a burst delay – flash duration relation.

I. INTRODUCTION

The transient sky is a treasure trove [1] of events and information about the energetic universe, ranging over gamma ray to radio wavelengths in light, plus neutrinos and gravitational waves, and over time scales from milliseconds to months. Well known cosmological examples include fast radio bursts (FRB) and gamma ray bursts (GRB) on millisecond to second timescales, binary black hole inspiral gravitational waves over milliseconds to days, and supernovae over days to months. Of course the entire universe can be viewed as transient over long enough timescales [2–7].

Time domain surveys specifically seek to explore the transient sky, with the next generation coming underway [8, 9]. Continuously scanning surveys can also detect transient events [10–13]. Multimessenger detection of an event in photons of diverse wavelengths, other high energy particles such as neutrinos or cosmic rays, or gravitational waves is a burgeoning new field, e.g. [14–18]. However, all these surveys tend to scan over seconds to days, insensitive to transients on shorter timescales. Certainly we know that astrophysical energetic events can occur down to nanosecond timescales, e.g. [19, 20]. Might optical surveys sensitive to subsecond timescales reveal a whole new world of events at cosmological distances?

Detector technology and imaging software is reaching capabilities to make such surveys a reality. In particular, the development of silicon photomultipliers (SiPM) with ultrafast readout and coincidence triggers [21, 22] may open up the era of Ultra Fast Astronomy, on millisecond and even submicrosecond timescales. Other detectors such as avalanche photodiodes [23] are also being explored. While they still have a long way to go in terms of large arrays, spatial resolution, and noise including crosstalk, they are capable of single photon detection and continuous readout.

Here, we will be particularly interested in detecting transients visible in multiple windows, e.g. gamma rays and optical light, or gravitational waves and optical light, and those that can be targeted, i.e. there is a precursor

or repeating event. This includes the search for optical counterparts of known energetic events, such as repeating fast radio bursts (FRB), delayed optical phenomena from a one time event, or even as part of an optical search for extraterrestrial intelligence (oSETI) program [24–26].

Given a large set of targets (e.g. prior burst locations), limited observing resources means that the time spent on each target looking for an optical flash must be optimized for a detection or characterization of the astrophysical process. This is the main topic of investigation here. Framed generally, given a set of adaptable observations, a merit function to optimize, a limited resource, and a cost function per observation, what is the best strategy. Astrophysically, this optimization analysis has been carried out for strong gravitational lens surveys [27] and supernova surveys (e.g. [28, 29]); for example, there the data set was the number of targets followed up at different redshifts, the merit function was the dark energy joint parameter estimation uncertainty (“figure of merit”), the limited resource the total spectroscopy time, and the cost function expressed the resource use of followup spectroscopic time by a target at redshift z . There may also be a systematics function that caps the number of useful targets in each observation (e.g. redshift) bin.

We investigate three separate science approaches. In Section II we begin by analyzing a simple two or three time bin optical followup program of repeating FRB, showing how to derive the optimal observing strategy. This gets expanded in Section III to a more realistic case, solved numerically, for not only detecting flashes but characterizing the underlying astrophysics through measuring abundances. Section IV presents a more physically incisive test of a property such as a burst delay – flash duration relation, possibly useful as a test of oSETI. We discuss further potential opportunities from technology development and conclude in Sec. V.

II. BURST OPTICAL COUNTERPARTS

We begin with a simple set up that allows analytic calculation, and focus on fast radio bursts as a concrete example, though the principles are generally applicable. Fast radio bursts are millisecond transients detected at radio wavelengths [30]. A fraction of them repeat, though not necessarily periodically. They may, however, have “active windows” that are periodic, with enhanced probability of a repeat burst sometime within the window. Determining whether FRB have optical emission, and measuring it, would be important for understanding the physics behind FRB; so far the millisecond timescale is too short to make such observations.

As an initial goal of Ultra Fast Astronomy we might seek to maximize the chances of detecting an optical counterpart, or the numbers of such burst counterparts that we will call flashes. Suppose the probability of a burst repeating a time t after a previous burst (so we know where to look) and having an optical counterpart (so there is something to detect) is some normalized $p_{\text{burst}}(t)$. Then in a window of time $[t_{i-1}, t_i]$ the probability of a viable repeat burst is

$$p_i(t_i) = \int_{t_{i-1}}^{t_i} dt p_{\text{burst}}(t). \quad (1)$$

This may be a function of burst properties, and we may later be interested in subtypes, but for now we simply consider any burst.

The observing procedure is taken to be a target list and assignment to observing time bins of various durations. For example, some targets we will observe for t_1 and if no flash is detected we move on to another target. Some targets we will observe for t_2 – if it does not flash by time t_2 we move on, if it flashes in the first t_1 time then we do not continue to observe it afterward, and place it in the bin corresponding to t_1 , and if it flashes between times t_1 and t_2 then it is in the bin corresponding to t_2 , etc.

The number of flashes detected is

$$N_{\text{flash}} = \sum_i N_{\text{target}}(t_i) p_i \equiv \sum_i n_i p_i. \quad (2)$$

where $n_i \equiv N_{\text{target}}(t_i)$ is the number of targets observed with time bin t_i (i.e. producing, or not, a flash between t_{i-1} and t_i). The question is whether we want a quick look at many targets or a long look at fewer targets – what is the optimum allocation?

In the case of limited resources, e.g. telescope time, we cannot observe as many targets as we want for as long as we want. Each observations comes with a cost, taking up part of the finite resources R . The cost function may be simply proportional to observing time, i.e. how much time we dedicate to searching for a flash from a target, so

$$R = \sum_i n_i t_i. \quad (3)$$

Combining these equations, we get

$$N_{\text{flash}} = p_1 \left[\frac{R}{t_1} - \sum_{i>1} n_i \left(\frac{t_i}{t_1} - \frac{p_i}{p_1} \right) \right]. \quad (4)$$

To maximize N_{flash} with respect to n_i , we evaluate the partial derivative, giving a critical condition

$$\frac{t_i}{t_1} = \frac{p_i}{p_1}. \quad (5)$$

There are three cases. One is that this has no solution because while by construction $t_i > t_1$, we may have $p_i < p_1$, depending on the form of $p_{\text{burst}}(t)$. In this case the quantity in parentheses in Eq. (4) is positive and so the maximum N_{flash} is when the sum goes to zero. That is, the optimum is to only observe on the shortest timescale, t_1 , with $n_{i>1} = 0$. A second case is when $p_i > p_1$ and $t_i/t_1 < p_i/p_1$. Then the subtracted sum gives a positive contribution and time bins beyond the shortest are useful. The third case is when $t_i/t_1 = p_i/p_1$, and this is interesting because it both fixes the time bins and leaves a degeneracy where a family of n_i gives the same optimum.

A simple model showing that an optimization can give a distribution, and not simply a preference for the shortest or the longest observation time, is $p_{\text{burst}}(t)$ of the form of a Gaussian centered at some time t_p , i.e. a FRB is likely to repeat at $t_p \pm \sigma$ after the last burst. Observing early or late is not preferred. We revisit this model later.

To study the three different cases, suppose we take the power law model

$$p_{\text{burst}}(t) = \frac{p_0 m}{t_c} \frac{(t/t_c)^{m-1}}{(t_{\max}/t_c)^m}, \quad (6)$$

so that

$$p_i = p_0 \frac{t_i^m - t_{i-1}^m}{t_{\max}^m}, \quad (7)$$

where t_{\max} is just a cutoff so p_{burst} is normalized to unity (really p_0) over $[0, t_{\max}]$. The critical point is when Eq. (5) holds. This gives a transcendental equation

$$\frac{t_i}{t_1} = \left(\frac{t_i}{t_1} \right)^m - 1. \quad (8)$$

It is convenient to define the time bin ratios $r_i = t_i/t_1$. Then our main equations for the probability model of Eq. (7) are

$$\frac{p_i}{p_1} = r_i^m - r_{i-1}^m \quad (9)$$

$$R = t_1 \sum_i n_i r_i \quad (10)$$

$$N_{\text{flash}} = p_1 \left[\frac{R}{t_1} + \sum_{i>1} n_i (r_i^m - r_i - r_{i-1}^m) \right]. \quad (11)$$

Case	Condition
$r_i < r_i^*$	0
$r_i = r_i^*$	degeneracy
$r_i^* < r_i \leq r_i^F$	0
$r_i > r_i^F$	maximum

TABLE I. Conditions for time bin i to be populated or not. 0 denotes it is unpopulated; degeneracy means that it is populated together with the $i-1$ bin and the numbers in each form a family along a linear combination degeneracy; maximum means that all bins $< i$ are unpopulated. The degeneracy and maximum conditions can be overridden by bins $> i$ such that bin i becomes unpopulated. The critical values r_i^* and r_i^F are defined in Eqs. (12) and (13).

The quantity in parentheses in N_{flash} will determine the critical values of r_i .

Suppose $m = 1$. Then there is no value where the parenthetical vanishes, and it is always negative: we always have $t_i/t_1 > p_i/p_1$ (i.e. $r_i > r_i - r_{i-1}$) and so the optimum is for all observations in the shortest time bin. However for $m > 1$ there can be positive, zero, or negative solutions.

We examine cases for some specific numbers of bins below, but present the summary here in Table I. The key criticality quantities (as we will see below) are

$$r_i^* \text{ solves } r_i^m - r_i - r_{i-1}^m = 0 \quad (12)$$

$$r_i^F \text{ solves } r_i^m - r_i \frac{r_{i-1}^m - r_{i-2}^m}{r_{i-1}} - r_{i-1}^m = 0. \quad (13)$$

A. $N = 2$ bins

Let us start by considering only two bins. Suppose also $m = 2$, so we can solve analytically the equation for the second bin to obtain the critical value $r_2^* = (1 + \sqrt{5})/2 = 1.618$, the golden ratio. If the time bin ratio r_2 is smaller than this critical value, we have the first case (observe only in the first bin); if it is larger we have the second case (observe in the second bin). When $r_2 = r_2^*$ (third case), then

$$N_{\text{flash}} = \frac{Rp_1}{t_1} = \frac{Rp_0 t_1^{m-1}}{t_{\max}^m}. \quad (14)$$

As an example, for $m = 2$, $t_1 = 1$, $t_{\max} = 10$, $p_0 = 1$, and $R = 1000$, with all times in common units, then $N_{\text{flash}} = 10$. However, note that for this case we are not free to choose t_2 but it is fixed to be $t_2 = r_2 t_1 = 1.618$. Moreover, we have a degenerate family

$$n_2 = \frac{R - n_1 t_1}{t_2} = \frac{1}{r_2} \left(\frac{R}{t_1} - n_1 \right), \quad (15)$$

along the line from $(n_1, n_2) = (1000, 0)$ to $(0, 618)$, all of which gives the same maximum N_{flash} (up to roundoff of an integer number of targets).

When $r_2 > r_2^*$ (and note for bin 2 that $r_2^* = r_2^F$), say $r_2 = 2$ for $m = 2$, then

$$N_{\text{flash}} = p_1 \left(\frac{R}{t_1} + n_2 \right), \quad (16)$$

with $p_2/p_1 = 3$, and since from R we can write

$$n_2 = \frac{R}{2t_1} - \frac{n_1}{2}, \quad (17)$$

then

$$N_{\text{flash}} = p_1 \left(\frac{3R}{2t_1} - \frac{n_1}{2} \right). \quad (18)$$

This is maximum for $n_1 = 0$ (i.e. observe only in the second bin) so $N_{\text{flash}} = 15$ and $n_2 = 500$.

When there are more than two time bins, the situation gets more complicated, and the critical condition must be evaluated for each bin. One solution is to choose the bins so that the critical condition holds for each bin and then $N_{\text{flash}} = p_1 R / t_1$. Since there is only one constraint equation $R(n_i)$ then this leaves a $N - 1$ fold degeneracy among N bins, generalizing Eq. (15).

B. $N = 3$ bins

Analyzing the $N = 3$ bin case gives a better sense of the various cases. The critical condition Eq. (8) applies to each bin i :

$$\frac{t_i}{t_1} \equiv r_i = \frac{p_i}{p_1} = r_i^m - r_{i-1}^m. \quad (19)$$

We again adopt $m = 2$ to enable analytic solutions and solve the quadratic to obtain

$$r_i^* = \frac{1 + \sqrt{1 + 4r_{i-1}^2}}{2}. \quad (20)$$

If the chosen value of t_i gives $r_i < r_i^*$ then the optimization removes all observations from bin i , i.e. $n_i = 0$. The higher bin critical values depend on the chosen values for the lower bins.

We already saw that $r_2^* = (1 + \sqrt{5})/2 = 1.618$. Thus, choosing $t_2 = 1.5t_1$, say, means $n_2 = 0$. Suppose we do choose $r_2 = 1.5$; then $r_3^* = 2.08$. So a sequence $\{t_1, t_2, t_3\} = \{1, 1.5, 2\}$ will optimize to all observations in the first bin, while $\{1, 1.5, 3\}$ will give all observations in the third bin. Taking $\{1, 1.5, 2.08\}$ will give observations in the first and third bins only, with a degeneracy condition in the division of numbers between them, as in Eq. (15). If we enable observations in the second bin by taking $r_2 = 2$ then $r_3^* = 2.56$. Choosing $r_3 = 2.5$ would mean all observations go in the second bin.

The situation with multiple $r_i > r_i^*$ is a little more involved: we need to take into account the resource weighting. Using

$$R = t_1 (n_1 + n_2 r_2 + n_3 r_3), \quad (21)$$

then Eq. (4) gives

$$N_{\text{flash}} = p_1 \left[R \frac{r_3^m - r_2^m}{r_3} + n_2 F(r_2, r_3) \right]. \quad (22)$$

(We have neglected the n_1 term because we know the optimization will give $n_1 = 0$, preferring either n_2 or n_3 since their r_i are above the critical value). The quantity

$$F \equiv r_2^m - 1 - \frac{r_2}{r_3} (r_3^m - r_2^m), \quad (23)$$

is important since if it is negative then the optimization gives $n_2 = 0$. The second two terms of F are negative, and if $m > 1$ then large r_3 guarantees negativity. So we need r_3 to be larger than its critical value but less than its F -critical value to allow for n_2 to contribute. For $m = 2$ we again get a quadratic equation with solution

$$r_3^F = \frac{r_2^2 - 1 + \sqrt{(r_2^2 - 1)^2 + 4r_2^4}}{2r_2}. \quad (24)$$

For example, for $r_2 = 2$ then $r_3^F = 2.886$.

Summarizing, when $r_3 < r_3^F$ then $F > 0$, and by Eq. (22) the optimization favors maximizing n_2 and setting $n_3 = 0$. When $r_3 > r_3^F$ then $F < 0$, and by Eq. (22) the optimization favors zeroing n_2 and maximizing n_3 (i.e. using the full resources R there). Only when $r_3 = r_3^F$ do we obtain optimized observations by having both second and third bins. In this case

$$N_{\text{flash}} = p_1 R \frac{(r_3^F)^m - r_2^m}{r_3^F} \quad (25)$$

$$= p_1 R \frac{r_2^m - 1}{r_2}. \quad (26)$$

That is, we have a continuity of the same optimum number N_{flash} for $r_3 = r_3^F$ as $r_3 < r_3^F$. One can readily verify that for $r_3 = 2.886$ and $r_2 = 2$ then indeed $N_{\text{flash}} = 15$. When $r_3 > r_3^F$ then

$$N_{\text{flash}} = p_1 R \frac{r_3^m - r_2^m}{r_3}. \quad (27)$$

While this appears like we can obtain many optical flashes by increasing r_3 without limit, we must recall that in this case $n_3 = R/r_3$ and so for a finite resource R we cannot increase r_3 beyond the point where $n_3 < 1$. In fact, since we have assumed one flash per target, we must have in this case $N_{\text{target}} = n_3 \geq N_{\text{flash}}$. Using $n_3 = R/r_3$ this gives

$$r_3^m \leq r_2^m + p_1^{-1} \quad (28)$$

$$r_3 \leq \left[r_2^m + p_0^{-1} \left(\frac{t_{\text{max}}}{t_1} \right)^m \right]^{1/m}, \quad (29)$$

since $p_1 = p_0(t_1/t_{\text{max}})^m$. This makes sense: r_3 is bounded by the maximum observing time allowed. In the limit $r_3 \approx p_0^{-1/m} t_{\text{max}}/t_1$,

$$N_{\text{flash}} = \frac{R p_0^{1/m} t_1}{t_{\text{max}}}, \quad (30)$$

which for our parameters gives $N_{\text{flash}} = 100$ (assuming $p_0 = 1$). The same formula is obtained if there are only two bins.

For such a probability as the power law form monotonically increasing with time, the longest observations are preferred. This also reduces the total number of targets observed, ameliorating issues with telescope slewing etc. However a peaked (e.g. Gaussian) probability distribution will have a different behavior. If one takes p_{burst} to be a Gaussian peaking at some time t_p then p_i will be a difference between error functions evaluated at t_i and t_{i-1} (see Sec. II D).

Finally, all three bins are enabled by choosing $r_2 = r_2^*$ and $r_3 = r_3^*(r_2^*)$. For $m = 2$ we have

$$r_2^* = \frac{1 + \sqrt{5}}{2} = 1.618 \quad (31)$$

$$r_3^*(r_2^*) = \frac{1 + \sqrt{7 + 2\sqrt{5}}}{2} = 2.194. \quad (32)$$

All three bins can contribute, with the triplet $\{n_1, n_2, n_3\}$ lying along the degeneracy line

$$R = n_1 + n_2 r_2^* + n_3 r_3^*(r_2^*), \quad (33)$$

and $N_{\text{flash}} = p_1 R$ for all such choices.

C. Constrained Optimization

While the formal optimal solution involves, basically, delta functions for specific observing times, this will tend to be blurred out by systematics or technical constraints (see e.g. [27]). For example, one may not want to slew the telescope to new targets so often and so want to cap the number of targets in the lowest time bin, or may want a diverse sample or one pushing the time frontier by reaching down to the instrumental time resolution, and so cap the number of targets in the highest time bin. Therefore we also analyze the optimization under the constraint of a cap of 30% of total resources placed on every bin.

Figure 1 presents the results for various choices of t_1 , t_2 , t_3 chosen without caps and so that caps force shifts of targets from the preferred bins to other bins. The numerical solution behavior follows the rules derived in the previous section and summarized in Table I: the next preferred bin is optimized according to the relation of r_i to r_i^* and r_i^F where appropriate. For example, in the two right panels the next preferred bin is the first bin in the top right panel since there $r_2 < r_2^*$, but the second bin in the bottom right panel since there $r_2 > r_2^*$. Any unexpended resources go into the least preferred of the three bins.

D. Gaussian Delay

To give another view of the optimization, where the preferred observing time is not at either extreme, we con-

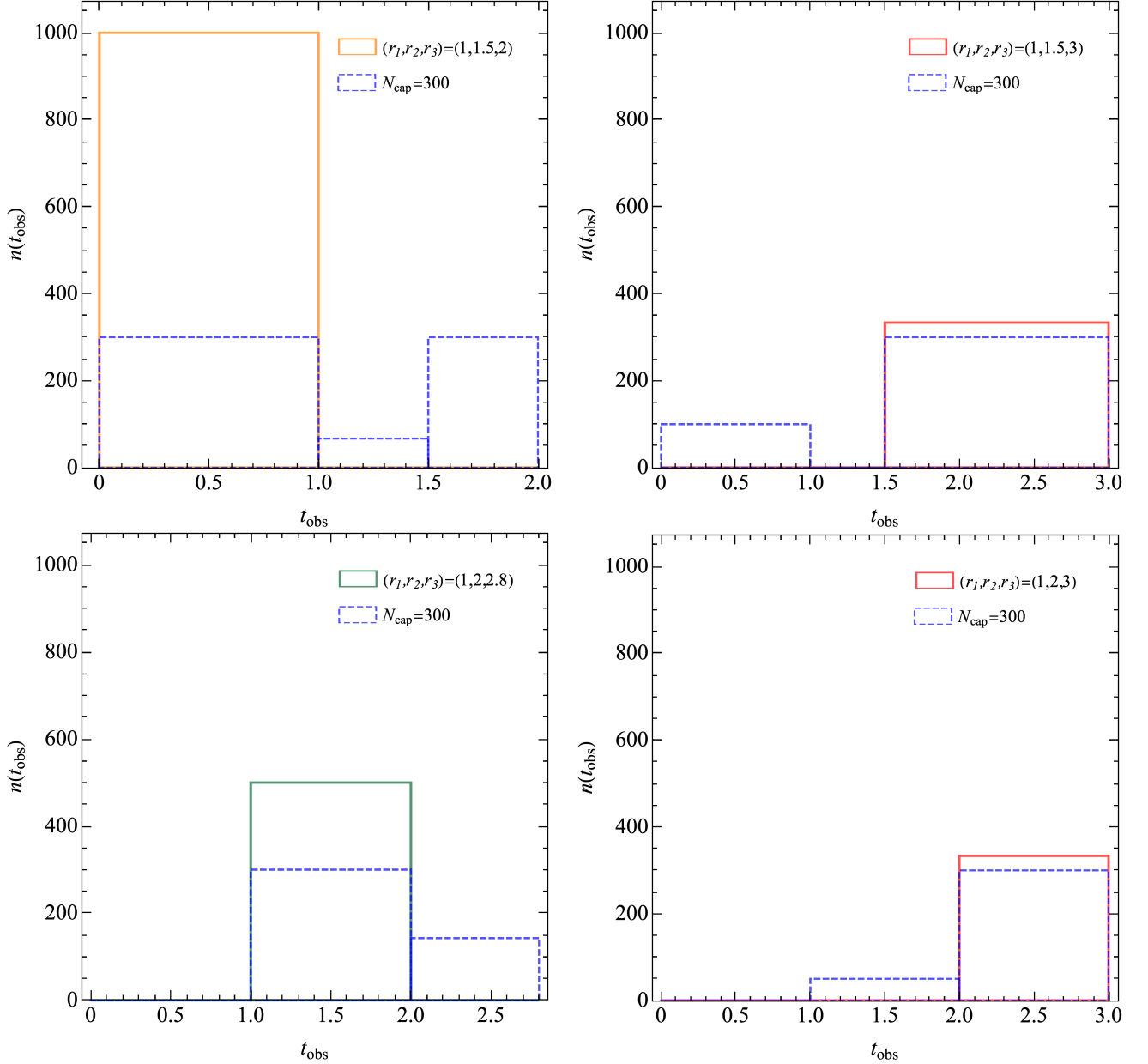


FIG. 1. The optimized observation time bin solutions $n(t_{\text{obs}})$ to maximize N_{flash} are plotted for various cases of r_1, r_2, r_3 for a power law burst probability Eq. (6). The different choices lie above or below the critical values r_i^*, r_i^F . Solid histograms show the unrestricted optimized case while dotted histograms impose a cap of 300 on any bin.

sider a Gaussian delay model. For

$$p_{\text{burst}}(t) = \frac{1}{\sqrt{2\pi}\sigma^2} e^{-(t-t_p)^2/(2\sigma^2)}, \quad (34)$$

this represents a burst that occurs a mean time t_p after time zero (e.g. the previous burst), but with some uncertainty σ . We will also use this in Secs. III and IV when we optimize determination of physical properties rather than merely numbers.

The probability for a flash within a window $[t_{i-1}, t_i]$ is

then

$$p_i(t_i) = \frac{1}{2} \left[\text{erf} \left(\frac{t_i - t_p}{\sigma\sqrt{2}} \right) - \text{erf} \left(\frac{t_{i-1} - t_p}{\sigma\sqrt{2}} \right) \right]. \quad (35)$$

We have the same criterion as before to decide whether to prefer bin i to bin j :

$$\frac{p_i}{p_j} > \frac{t_i}{t_j}. \quad (36)$$

In particular, if $j = 1$ and the condition is violated then the optimization prefers the shortest time bin – this was

the r_i^* criterion. If $j = i - 1$ and the condition holds, then the optimization prefers the longer time bin (unless it is overruled by an even higher bin) – this was the r_i^F criterion.

Figure 2 shows the optimization results for several cases. As before, a single time bin is preferred (this is fairly generic when dealing with one free parameter [28], here N_{flash}). The exact time bin preferred is a function of t_p and σ (and the bin width), but the solution is not analytic as Eq. (36) involves error functions. When σ is small enough, the preferred observation time should be near the mean time t_p , but it moves to earlier time bins for larger σ , and then will jump to the lowest bin once the error function ratio falls below the linear time ratio in Eq. (36).

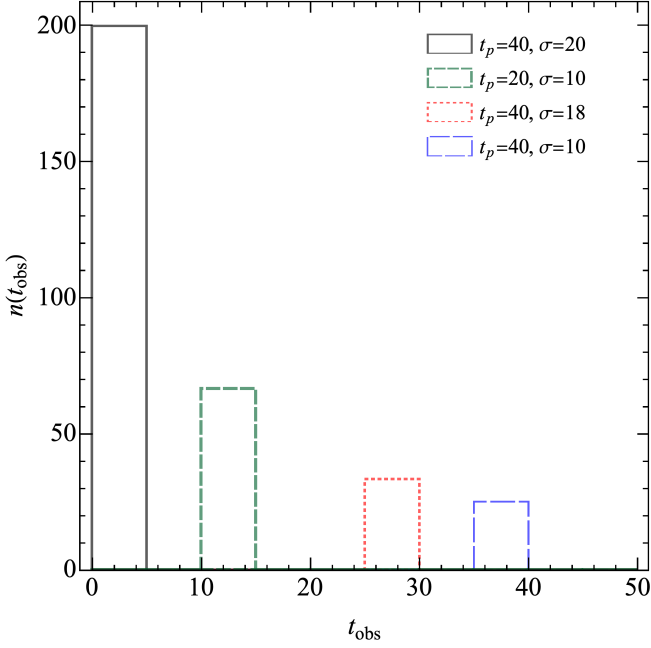


FIG. 2. The observation time solutions optimized for N_{flash} , given constant resources, when p_{burst} follows a Gaussian form with mean t_p and standard deviation σ . The solutions prefer a single time bin; we show four cases, labeled with t_p and σ . Time bins have constant widths of 5 (in the same units as the resource $R = 1000$) and no caps are placed on the number per bin.

III. DELAY-DURATION RELATION – VIA ABUNDANCE

While detecting ultra fast optical transient counterparts would be exciting and significant, it would be even better to extract some physics out of the detections. As one illustration, suppose the optical flash durations scale with some power of the burst delay t_p . We write

$$\tau = At_{\star} \left(\frac{t_p}{t_{\star}} \right)^s, \quad (37)$$

where t_{\star} is a fixed pivot scale, A is the dimensionless amplitude of the relation (with a t_{\star} out front for correct dimensionality) and s is the slope relating the mean burst delays to the flash durations. This could be relevant to the astrophysical bursting mechanism, e.g. of FRB or GRB, and also to oSETI, where a civilization might choose to broadcast short messages frequently, or long messages infrequently, in a sort of constant energy output schema.

We will use a Fisher information matrix approach to determining the physical parameters A and s from the flash detections, and then optimizing the observation time distribution to get the best constraints. In this section we take the observable to be the number of flashes in a certain observation time bin t_i (as before), summed over the flash durations τ . We want to relate these measured abundances to the underlying process parameters of the burst delay t_p and delay-duration slope s . (In Section IV we take a more direct approach.)

We begin with the number of flashes detected in the observation time bin i : $t_{i-1} < t_{\text{obs}} < t_i$, with duration τ . A subscript i means such a time bin and we take all bins to be of equal, unit width. Then

$$N_{\text{flash}}(t_i; \tau) = n_{\text{burst}}(t_i) p_{\text{flash}}(t_i; \tau) \quad (38)$$

$$= n_{\text{burst}}(t_i) p_{\text{flash}}(t_i; t_p) \left| \frac{dt_p}{d\tau} \right|, \quad (39)$$

where we used $p_{\text{flash}}(t_i; \tau) d\tau = p_{\text{flash}}(t_i; t_p) dt_p$. The quantity $p_{\text{flash}}(t_i; t_p)$ is given by Eq. (35). Using the inverse of Eq. (37),

$$t_p = t_{\star} \left(\frac{\tau}{At_{\star}} \right)^{1/s}, \quad (40)$$

we can calculate the Jacobian

$$J \equiv \left| \frac{dt_p}{d\tau} \right| = \frac{1}{As} \left(\frac{\tau}{At_{\star}} \right)^{(1-s)/s}. \quad (41)$$

Explicitly,

$$N_{\text{flash}}(t_i; \tau) = n_{\text{burst}}(t_i) p_{\text{flash}}(t_i; t_p(\tau, A, s)) \times \frac{1}{As} \left(\frac{\tau}{At_{\star}} \right)^{(1-s)/s}. \quad (42)$$

To carry out the Fisher information analysis, we need the sensitivities: the derivatives with respect to the parameters,

$$\frac{\partial N_{\text{flash}}(t_i, \tau)}{\partial A}, \quad \frac{\partial N_{\text{flash}}(t_i, \tau)}{\partial s}. \quad (43)$$

Note that

$$\frac{\partial p_i(t_p(\tau, A, s))}{\partial \theta} = \frac{\partial p_i(t_p(\tau, A, s))}{\partial t_p} \frac{\partial t_p}{\partial \theta}, \quad (44)$$

for $\theta = \{A, s\}$ and $p_i(t_p) \equiv p_{\text{flash}}(t_i; t_p)$. The derivatives

$$\frac{\partial t_p}{\partial A} = \frac{-t_p}{sA}, \quad \frac{\partial t_p}{\partial s} = \frac{-t_p}{s^2} \ln \left(\frac{\tau}{At_{\star}} \right), \quad (45)$$

and for the Jacobian factor

$$\frac{\partial J}{\partial A} = \frac{-J}{sA}, \quad \frac{\partial J}{\partial s} = \frac{-J}{s^2} \left[s + \ln \left(\frac{\tau}{At_*} \right) \right]. \quad (46)$$

Putting it all together,

$$\frac{\partial N_{\text{flash}}(t_i, \tau)}{\partial A} = \frac{-N_{\text{flash}}}{sA} \left[\frac{t_*}{p_i(t_p)} \frac{dp_i}{dt_p} \left(\frac{\tau}{At_*} \right)^{1/s} + 1 \right], \quad (47)$$

and

$$\begin{aligned} \frac{\partial N_{\text{flash}}(t_i, \tau)}{\partial s} &= \frac{-N_{\text{flash}}}{s^2} \left[\frac{t_*}{p_i(t_p)} \frac{dp_i}{dt_p} \left(\frac{\tau}{At_*} \right)^{1/s} \ln \left(\frac{\tau}{At_*} \right) \right. \\ &\quad \left. + s + \ln \left(\frac{\tau}{At_*} \right) \right], \end{aligned} \quad (48)$$

where the derivative is evaluated at $t_{p,\text{fid}} = t_*(\tau/At_*)^{1/s}$. For $p_i(t_p)$ given by Eq. (35), its derivative is a difference between Gaussians; the $1/p_i(t_p)$ term cancels the $p_i(t_p)$ in N_{flash} .

We also need to specify the measurement noise matrix, e.g. Poisson measurement error on the abundances so that $C^{-1} = N_{\text{flash}}(t_i, \tau)$, and the fiducial values, e.g. $s = 1$ and $A = 1/4$, with a pivot scale $t_* = 40$. The Fisher information matrix is summed over the bins in τ – with the constraint that $\tau < t_i$ (we can't measure a duration longer than we have observed for) – and then summed over bins in observing time t_i . Thus,

$$F_{pq} = \sum_{\text{bins of } t_i} \sum_{\text{bins with } \tau < t_i} \frac{\partial N_{\text{flash}}(t_i, \tau)}{\partial \theta_p} \frac{\partial N_{\text{flash}}(t_i, \tau)}{\partial \theta_q} N_{\text{flash}}(t_i, \tau). \quad (49)$$

Figure 3 shows $N_{\text{flash}}(t_i, \tau)$ and the Fisher sensitivities $\partial \ln N_{\text{flash}}/\partial \theta$ for our parameters, $\theta = A$ and s . We see the sensitivity curves vs the flash duration τ have very different shapes, implying little covariance is expected in their determination. Both the delay-duration amplitude A and slope s should be well determined if we observe a range of durations.

Figure 4 illustrates the Fisher information analysis results for the parameter uncertainties and the figure of merit $(\det F)^{1/2}$ related to the inverse area of the amplitude–slope confidence contour. We see that the slope is determined at about the same level for $t_{\text{obs}} \gtrsim 10$ while the amplitude is best determined near the pivot scale $t_* = 40$. Due to the changing covariance between the parameters, however, the figure of merit (FOM) ends up being monotonic, gaining more information with a longer observation time.

Figure 5 shows the joint 1σ confidence contours for three different values of t_{obs} . As expected from Fig. 4, the estimation of the slope s changes little, but the probability ellipse rotates to give a smaller range for amplitude A near $t_i = 40$, thinning the ellipse as t_i increases, giving a smaller area and larger FOM.

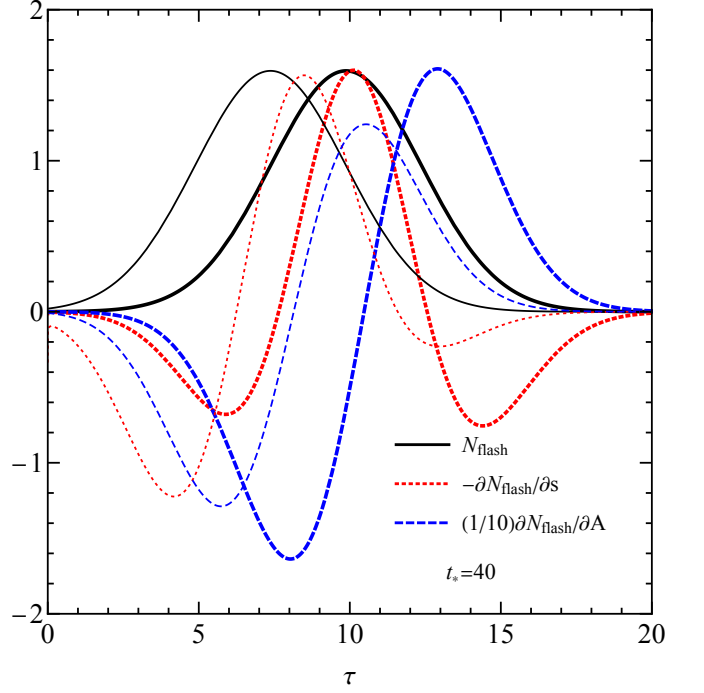


FIG. 3. The Fisher sensitivities $\partial N_{\text{flash}}/\partial \theta$ (dotted red for s , dashed blue for A) have very different shapes, i.e. dependence on the observed flash duration τ , so we may expect little covariance between them, allowing both to be well estimated from data. The solid black curves show $N_{\text{flash}}(t_i, \tau)$. Bolder curves are for $t_i = 40$, thinner curves are for $t_i = 30$.

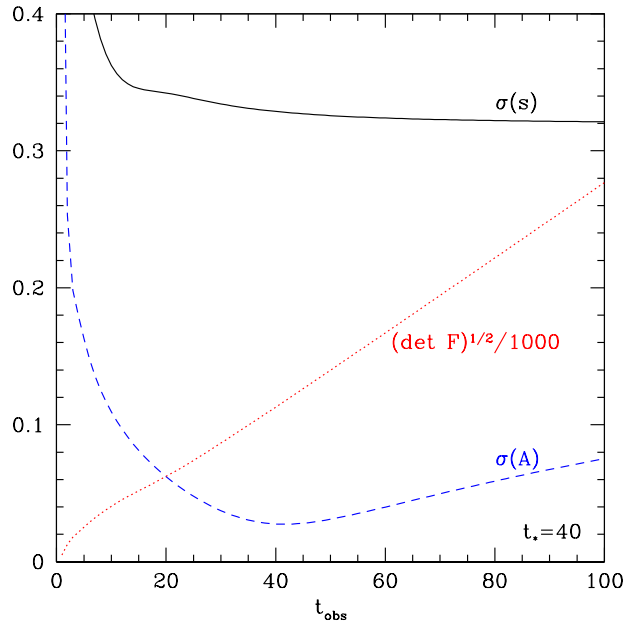


FIG. 4. Parameter estimation and figure of merit as a function of observing time bin $t_i \equiv t_{\text{obs}}$. For all bins $n_i = 10$ here.

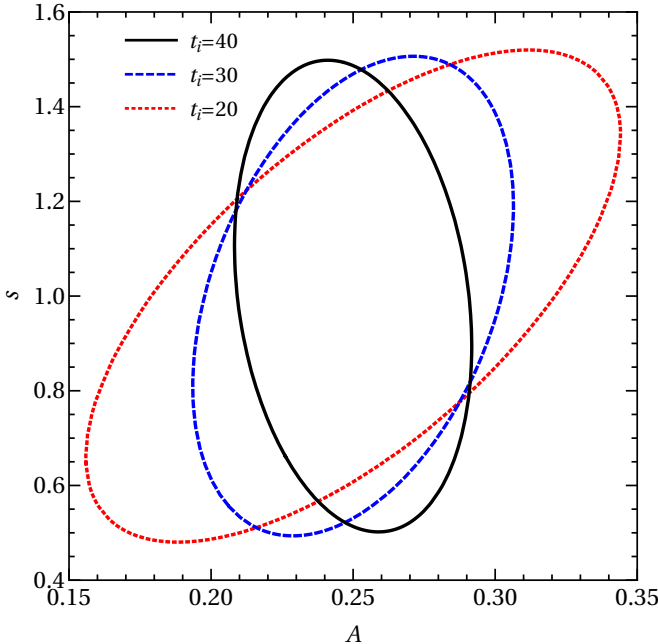


FIG. 5. Joint probability contours (68.3% confidence level) for the amplitude A and slope s , for three different values of observing time bin t_i . For all bins $n_i = 10$ here.

For the full Fisher information analysis, one sums over the whole range of observing time bins t_i , weighted by the number of targets in that bin, n_i . This will of course reduce the uncertainties on the parameter estimation. However our main aim is to determine the optimum observing strategy, i.e. the optimum distribution n_i , under our observing time resource constraint and cost model.

We use two independent codes to carry out the optimization. One is the Fisher optimization code described in [27], adapted for the present observables and variables, that evaluates the change in merit with resource unit (observing time), bin by bin, selects the bin with weakest leverage, reduces that n_i , and reallocates its time to other bins (hence changing n_j) in a fashion weighted by the merit per resource used. The other uses the interior point optimization algorithm which combines the resource constraint and the merit function using the barrier function approach [31]. They provide valuable crosschecks on results and convergence.

The results show the optimization favors maximum numbers in the lowest observation time bin, due to the resource constraint. While FOM improves with t_{obs} , lower t_{obs} allows many more targets within the given resource constraint. Since the Fisher information basically goes as n_i^3 (two factors from the observable N_{flash} proportional to n_i and one from the Poisson noise model), putting all observations in the lowest t_{obs} bin wins. Of course there may be other constraints limiting the number of targets, such as from available repeaters, the telescope, detectors, etc. In that case, the optimum found fills up the lowest bin to the maximum allowed, proceeds to the next lowest

bin, and so forth until the resource allotment runs out.

A short analytic proof of the behavior comes from considering the FOM if all observing is in bin p vs $q > p$. In the first case, $FOM = cn_p^3 p$, where from Fig. 4 we approximate the dependence of FOM on t_{obs} as roughly linear. In the second case $FOM' = cn_q^3 q$, but the resource constraint imposes that $n_q = n_p p/q$. Therefore we have $FOM' = FOM (p/q)^2 < FOM$ since $p < q$. Thus the lower bin always wins for this model with the abundance as the main observable.

IV. DELAY-DURATION RELATION – VIA DIRECT MEASUREMENT

The optimization in the previous section led to an all or nothing result: the solution involved fitting from target to target as fast as possible to observe as many as one could within the resource constraint. This was driven by the strong dependence of the Fisher information on the number of events, due to taking the abundance as the central observable. A more subtle, and interesting, result comes if the observable is the flash duration itself, in deriving the relation to the burst delay. We analyze this case here.

The Fisher information matrix now becomes

$$F_{jk} = \sum_{t_i} \sum_{\tau < t_i} \frac{\partial \tau}{\partial \theta_j} \frac{\partial \tau}{\partial \theta_k} N_{\text{flash}}(t_i, \tau) C^{-1} \quad (50)$$

$$= \sum_{t_i} n_i \sum_{\tau < t_i} \frac{\partial \tau}{\partial \theta_j} \frac{\partial \tau}{\partial \theta_k} p(t_i, t_p(\tau)) \left| \frac{dt_p}{d\tau} \right| C^{-1}, \quad (51)$$

where C is the measurement noise matrix. The sensitivities are

$$\frac{\partial \tau}{\partial A} = \frac{\tau}{A}, \quad \frac{\partial \tau}{\partial s} = \frac{\tau}{s} \ln \left(\frac{\tau}{At_*} \right), \quad (52)$$

the Jacobian $|dt_p/d\tau|$ is given by Eq. (41), and for C we take a diagonal matrix with elements $C = \sigma_\tau^2 \delta_{qq}$ where q is the index for the τ bin and

$$\sigma_\tau^2 = \sigma_{\text{stat}}^2 + N_{\text{flash}}(t_i, \tau) \sigma_{\text{sys}}^2. \quad (53)$$

The statistical contribution may depend on τ , though we take a fiducial case $\sigma_{\text{stat}} = 1$, and the systematic imposes a floor on the measurement uncertainty, or ceiling on the number of events such that increasing their quantity does not significantly add to the Fisher information beyond some limit (i.e. it cancels the $N_{\text{flash}}(t_i, \tau)$ in the numerator of F_{jk} : effectively, instead of a measurement uncertainty $\sigma_{\text{stat}}/\sqrt{N_{\text{flash}}}$ one has σ_{sys}). We investigate two fiducials $\sigma_{\text{sys}} = 0$ or 1.

We start the optimization from an initial state of uniform n_i across all bins $t_i = [1, 100]$, giving a fixed resource constraint of $R = 5050$. First we take a purely statistical uncertainty, with $\sigma_{\text{stat}} = 1$. Parameter estimation results will scale linearly with this, and as the reciprocal square root of the total resources available; however it will not

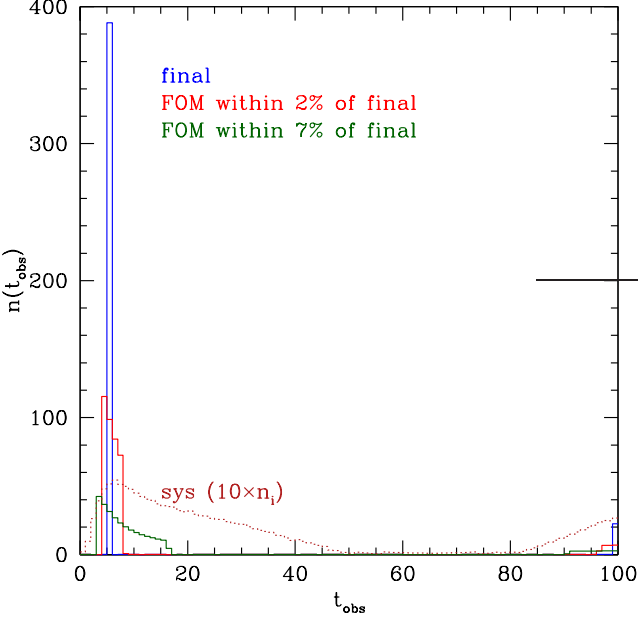


FIG. 6. Histogram of the optimized target distribution n_i , producing the maximum FOM under a fixed resource constraint. The solid histograms are for a purely statistical measurement uncertainty of $\sigma_{\text{stat}} = 1$. Distribution results n_i are shown for three different stages in the optimization process approaching the final convergence having sharp peaks at $t_i = 6$ and $t_i = 100$. Parameter constraints generally have smaller deviations from their final values than that listed for FOM. The dotted brown curve shows the impact of turning on a systematic, with $\sigma_{\text{sys}} = 1$, where the optimized histogram is plotted at ten times its true height (i.e. really $n_i < 6$).

affect the form of the distribution optimization for n_i (for σ_{stat} independent of τ). The final converged optimization gives two peaks in the n_i target distribution, at $t_i \approx 6$ and 100, as seen in Fig. 6. Note [28] also found that for a system with P parameters the distribution is optimized with P delta functions. The numerical solution approaches isolated peaks, with earlier iterations having slightly broader peaks, but these have nearly the final parameter uncertainties and FOM so we see that small variations in the distribution (e.g. due to observational requirements) have only a minor impact on the science results.

A systematic measurement uncertainty on τ , given by σ_{sys} , will place a ceiling on the number of productive targets in a given observing bin t_i . This flattens the distribution peaks, broadening them and distributing the targets over many more bins. Including the systematics in quadrature, with $\sigma_{\text{sys}} = 1$, worsens the parameter estimation by 22% on A and 44% on s , and by 33% on FOM.

We study the sensitivity of the FOM to the fiducial parameters in Fig. 7. Our fiducial value for the slope, $s = 1$, is seen to be the most conservative choice: other values of s give a higher FOM and tighter parameter estimation.

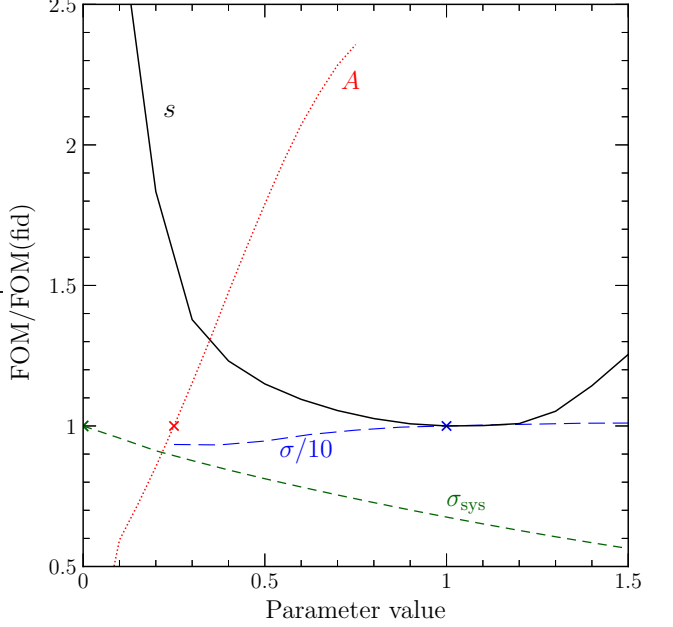


FIG. 7. The change of FOM relative to the fiducial result is plotted vs the parameter values away from their fiducials (marked with x's): $s_{\text{fid}} = 1$, $A_{\text{fid}} = 0.25$, $\sigma = 10$, $\sigma_{\text{sys}} = 0$. To keep σ on the same scale the x-axis is $\sigma/10$; note we cut off the curve for small σ as it approaches the time bin width. For A we cut off the curve as the flash duration approaches the burst delay time $A = 1$, otherwise it would not be a flash but a continuous glow.

This makes sense in that, broadly, when $s = 1$ some parameter dependence does not enter, e.g. in Eq. (41) and hence N_{flash} . More specifically, for smaller s we also amplify the sensitivity $\partial\tau/\partial s$ and increase the Jacobian $dt_p/d\tau$. Thus we expect small s to show the greatest improvement in parameter constraints and FOM. What we find for $s > 1$ is that, while the parameter constraints weaken, the FOM increases since there is less covariance between parameters – this is due to the enhanced range of τ contributing to a given favored t_p near t_i from the $1/s$ exponent in the relation Eq. (40).

For the amplitude A , the main effect is that larger τ is preferred for a given t_p near t_i . Since the sensitivities strengthen with increased τ , and the Fisher information goes as the product of sensitivity factors, this overcomes the reduced $dt_p/d\tau$. In fact, since $\partial\tau/\partial s$ is the only sensitivity benefiting (with the increase in A and τ canceling in $\partial\tau/\partial A$), the improvement in the estimation of s and in FOM is roughly linear in A , while the estimation of A weakens slightly. (Only FOM is shown in Fig. 7.)

Increasing the systematic σ_{sys} of course decreases FOM and worsens the parameter estimation. The uncertainty in the burst wait time σ has a minor effect, since it only enters into the probability factor and not the Fisher sensitivities. Decreasing σ makes it a little harder for t_i to match t_p , but we can still find some t_i matching t_p , where

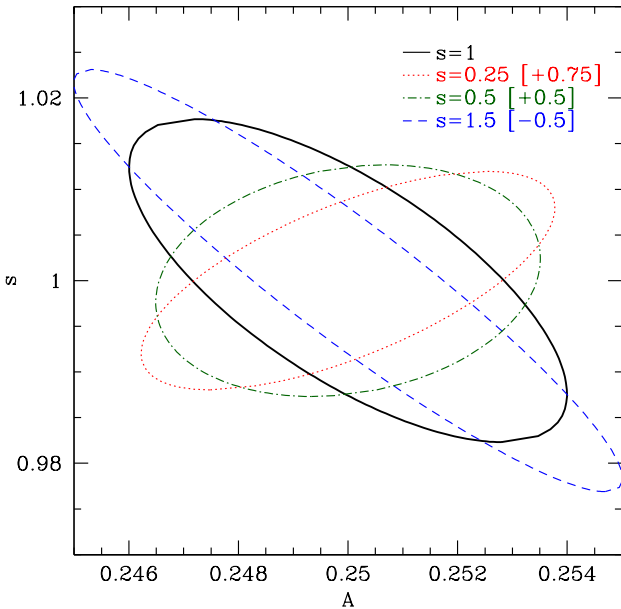


FIG. 8. 1σ joint confidence contours in the A - s plane, for different fiducial values of s . Constraints are for statistical uncertainties only with $\sigma_{\text{stat}} = 1$. Contours have been shifted vertically by the amount in brackets so that all are centered at $s = 1$, for easier comparison, despite the different fiducial values for s .

the probability is maximal.

Figure 8 shows how the parameter constraints evolve as we change the fiducial slope s , as well as the impact on the FOM (inverse area of the confidence contour). In particular, we can see how for $s = 1.5$, although the individual parameter constraints are weaker, the FOM is higher due to the narrowing of the joint contour. As the fiducial s changes, the covariance between A and s does as well, rotating the contour and squeezing or broadening it. The slope and amplitude of the burst delay – flash duration relation can be determined at the percent level, for the resources assumed. Such a result is promising for testing an oSETI hypothesis of constant energy output, i.e. $\tau/t_p = \text{constant}$, or $s = 1$. Since this plot is with statistical uncertainties only, the constraints scale with resources: linearly for FOM and as the inverse square root for the parameter estimation uncertainties.

V. CONCLUSIONS

Ultra Fast Astronomy can uncover a new view of the universe, unknown to those scanning celestial sources on

time scales of seconds or longer. Technology such as photomultipliers and photodiodes is approaching the capability of millisecond, microsecond, or even nanosecond resolution in the optical time domain.

This may reveal not only new classes of transients, but connections between transients across wavelengths and multimessenger signals. Such detections could provide critical clues to the physical origins and mechanisms behind highly energetic events – or even hints in the search for extraterrestrial intelligence.

We explore three cases of optimizing observations so as to maximize science under constrained resources, such as telescope time. First we simply look to optimize the number of counterpart detections, and solve analytically a toy model of how to distribute search durations before moving to another target. We then investigate science characterization from counterpart (flash) detection, such as testing a burst delay – flash duration relation. We analyze optimizations in terms of measured abundances, and then using measured flash durations. The study includes interpretation of the parameter estimation constraints and figure of merit (inverse area of the joint confidence contour), scaling with intrinsic and survey parameter values, and role of statistical and systematic uncertainties.

Under constrained resources, the derived optimum is a two prong observational strategy of many targets observed for a short (but not minimal) time and a few targets observed for a (maximally) long time. Resulting parameter estimation can reach the percent level. For example, a “constant energy output” schema of extraterrestrial signaling could be measured at signal to noise $S/N \approx 100$ for our fiducial resource level.

These are examples of survey strategy and science analysis that could be useful for Ultra Fast Astronomy. A considerable number of other investigations and multimessenger relations could be enabled by and assessed for Ultra Fast Astronomy. Future work also includes connecting the measurement uncertainty model more closely with promising detector technology characteristics.

ACKNOWLEDGMENTS

We thank Albert Wai Kit Lau for helpful discussions. This work is supported in part by the Energetic Cosmos Laboratory. EL is supported in part by the U.S. Department of Energy, Office of Science, Office of High Energy Physics, under contract no. DE-AC02-05CH11231.

[1] S.D. Wyatt, A. Tohuvavohu, I. Arcavi, M.J. Lundquist, D.A. Howell, D.J. Sand, The Gravitational Wave Treat-

sure Map: A Tool to Coordinate, Visualize, and Assess the Electromagnetic Follow-Up of Gravitational

- Wave Events, *Astrophys. J.* 894, no.2, 127 (2020) [[arXiv:2001.00588](#)].
- [2] A. Stebbins, Measuring Space-Time Geometry over the Ages, *Int. J. Mod. Phys. D* 21, 1242017 (2012) [[arXiv:1205.4201](#)].
- [3] D. Erskine et al. Direct Acceleration: Cosmic and Exoplanet Synergies, [[arXiv:1903.05656](#)].
- [4] A.G. Kim, E.V. Linder, J. Edelstein and D. Erskine, Giving Cosmic Redshift Drift a Whirl, *Astropart. Phys.* 62, 195-205 (2015) [[arXiv:1402.6614](#)].
- [5] O.H. Marcori, C. Pitrou, J.-P. Uzan, T.S. Pereira, Direction and redshift drifts for general observers and their applications in cosmology, *Phys. Rev. D* 98, no.2, 023517 (2018) [[arXiv:1805.12121](#)].
- [6] J. Bel and C. Marinoni, Proposal for a Real-Time Detection of our Acceleration through Space, *Phys. Rev. Lett.* 121, no.2, 021101 (2018) [[arXiv:1802.04495](#)].
- [7] C. Quercellini, L. Amendola, A. Balbi, P. Cabella and M. Quartin, Real-time Cosmology, *Phys. Rept.* 521, 95-134 (2012) [[arXiv:1011.2646](#)].
- [8] E.C. Bellm et al. The Zwicky Transient Facility: System Overview, Performance, and First Results, *Publ. Astron. Soc. Pac.* 131, 018002 (2019) [[arXiv:1902.01932](#)].
- [9] LSST Dark Energy Science Collaboration, The LSST Dark Energy Science Collaboration (DESC) Science Requirements Document, [[arXiv:1809.01669](#)].
- [10] S. Naess et al. The Atacama Cosmology Telescope: Detection of mm-wave transient sources, [[arXiv:2012.14347](#)].
- [11] K. Abazajian et al. CMB-S4 Science Case, Reference Design, and Project Plan, [[arXiv:1907.04473](#)].
- [12] A. Slosar et al. Packed Ultra-wideband Mapping Array (PUMA): A Radio Telescope for Cosmology and Transients, [[arXiv:1907.12559](#)].
- [13] N. Whitehorn et al. Millimeter Transient Point Sources in the SPTpol 100 Square Degree Survey, *Astrophys. J.* 830, no.2, 143 (2016) [[arXiv:1604.03507](#)].
- [14] V. Kalogera et al. The Yet-Unobserved Multi-Messenger Gravitational-Wave Universe, [[arXiv:1903.09224](#)].
- [15] M.J. Dyer et al. The Gravitational-wave Optical Transient Observer (GOTO), *Proc. SPIE Int. Soc. Opt. Eng.* 11445, 114457G (2020) [[arXiv:2012.02685](#)].
- [16] G. Hallinan et al. The DSA-2000 – A Radio Survey Camera, [[arXiv:1907.07648](#)].
- [17] J.P. Blakeslee et al. Probing the Time Domain with High Spatial Resolution, *Bulletin of the AAS*, 51(3), [[arXiv:1903.08184](#)].
- [18] M.M. Kasliwal et al. The Dynamic Infrared Sky, [[arXiv:1903.08128](#)].
- [19] A. Philippov, D.A. Uzdensky, A. Spitkovsky and B. Cerutti, Pulsar Radio Emission Mechanism: Radio Nanoshots as a Low Frequency Afterglow of Relativistic Magnetic Reconnection, *Astrophys. J. Lett.* 876, no.1, L6 (2019) [[arXiv:1902.07730](#)].
- [20] A. Stebbins, H. Yoo, Are Crab Nanoshots Schwinger Sparks?, [[arXiv:1505.06400](#)].
- [21] A.W.K. Lau, M. Shafiee, G.F. Smoot, B. Grossan, S. Li, Z. Maksut, On-sky silicon photomultiplier detector performance measurements for millisecond to sub-microsecond optical source variability studies, *JATIS* 6(4), 046002 (2020) [[arXiv:2002.00147](#)].
- [22] S. Li, G.F. Smoot, B. Grossan, A.W.K. Lau, M. Bekbalanova, M. Shafiee, T. Stetzelberger, Program objectives and specifications for the Ultra-Fast Astronomy observatory, *Proc. SPIE* 11341, Space Optics, Telescopes, and Instrumentation, 113411Y (2019) [[arXiv:1908.10549](#)].
- [23] S. Li, J. Maire, M. Cosens, and S.A. Wright, Detector characterization of a near-infrared discrete avalanche photodiode 5x5 array for astrophysical observations, *Proc. SPIE* 11002, Infrared Technology and Applications XLV, 110022G (2019) [[arXiv:1906.03837](#)].
- [24] S.A. Wright et al. Panoramic optical and near-infrared SETI instrument: overall specifications and science program, *Proc. SPIE* 10702, Ground-based and Airborne Instrumentation for Astronomy VII, 107025I (2018) [[arXiv:1808.05772](#)].
- [25] D.M. Kipping, A. Teachey, A cloaking device for transiting planets, *MNRAS*, 459, 1233 (2016) [[arXiv:1603.08928](#)].
- [26] J.R.A. Davenport, SETI in the Spatio-Temporal Survey Domain, [[arXiv:1907.04443](#)].
- [27] E.V. Linder, Tailoring Strong Lensing Cosmographic Observations, *Phys. Rev. D* 91, 083511 (2015) [[arXiv:1502.01353](#)].
- [28] D. Huterer, M.S. Turner, Probing the dark energy: methods and strategies, *Phys. Rev. D* 64, 123527 (2001) [[arXiv:astro-ph/0012510](#)].
- [29] J.A. Frieman, D. Huterer, E.V. Linder, and M.S. Turner, Probing Dark Energy with Supernovae: Exploiting Complementarity with the Cosmic Microwave Background, *Phys. Rev. D* 67, 083505 (2003) [[arXiv:astro-ph/0208100](#)].
- [30] E. Petroff, J.W.T. Hessels, D.R. Lorimer, Fast Radio Bursts, *Astron. Astroph. Rev.* 27, 4 (2019) [[arXiv:1904.07947](#)].
- [31] E.W. Weisstein, Interior Point Method. From MathWorld—A Wolfram Web Resource. <https://mathworld.wolfram.com/InteriorPointMethod.html>